Direct demonstration of decoupling of spin and charge currents in nanostructures

M. Urech, V. Korenivski, N. Poli, & D. B. Haviland

Nanostructure Physics, Royal Institute of Technology, 10691 Stockholm, Sweden

Abstract

The notion of decoupling of spin and charge currents is one of the basic principles underlying the rapidly expanding field of Spintronics. However, no direct demonstration of the phenomenon exists. We report a novel measurement, in which a non-equilibrium spin population is created by a point-like injection of current from a ferromagnet across a tunnel barrier into a one dimensional spin channel, and detected differentially by a pair of ferromagnetic electrodes placed symmetrically about the injection point. We demonstrate that the spin current is strictly isotropic about the injection point and, therefore, completely decoupled from the uni-directional charge current.

Each individual electron in a conductive material transports a quantum of charge as well as a quantum of spin. This charge-spin coupling, fundamental for individual electrons, is generally broken for ensembles of electrons. For the ensemble, spin is not conserved because spin-flip scattering provides a means of reversing the spin of the electron. No comparable mechanism exists for changing the charge of the electron, and charge is strictly conserved. Even though the notion of spin-charge decoupling of currents [1] is one of the basic concepts underlying the rapidly expanding field of Spintronics [2], no direct demonstration of the phenomenon exists and controversies persist [3, 4, 5, 11, 12]. We report a novel measurement, in which a non-equilibrium spin population is created by a point-like injection of current from a ferromagnet across a tunnel barrier into a metallic nanowire, and detected differentially by a pair of ferromagnetic electrodes placed symmetrically about the injection point. We demonstrate that the spin current in the wire is strictly isotropic about the injection point and therefore completely decoupled from the uni-directional charge current. This device creates an ideal source of pure spin current that can be easily controlled by the geometry of the device. This general concept of 'spin pumping' is currently of great fundamental and technological interest, forming the base for new types of spintronic devices [6].

Fundamental to the rapidly growing field of Spintronics is the ability to manipulate spin currents in nanostructures, which promises new implementations of memory and logic [2]. The first suggestions on spin injection and its detection date back a few decades [8, 1]. A spin polarized current,

$$j_s \equiv j_\uparrow - j_\downarrow \equiv \gamma(j_\uparrow + j_\downarrow) \equiv \gamma j_q,$$

injected form a ferromagnet (F) into a nonmagnetic conductor (N) creates a spin splitting of the chemical potential at the F/N interface, which is directly determined by the spin polarization of the injected current, γ,

$$\bigtriangledown\delta\mu \equiv \bigtriangledown(\mu_\uparrow - \mu_\downarrow) = e\rho_N \mathbf{j}_s = e\rho_N \gamma \mathbf{j}_q.$$

Here ρ_N is the resistivity of N and e is the electron charge (j_s and j_q are collinear at the injection interface). This non-equilibrium spin population decays away from the injection point into N over a characteristic spin flip length λ_{sf}, and is governed by a diffusion equation

$$\bigtriangledown^2 \delta\mu(\mathbf{r}) = \frac{1}{\lambda_{sf}^2}\delta\mu(\mathbf{r}). \tag{1}$$

It is essential to realise that the spin and charge currents are generally decoupled everywhere in N except at the injection point. This is easily illustrated by writing out the spin-up and spin-down currents in N using $\mu_{\uparrow,\downarrow}(\mathbf{r}) \equiv \mu_0 \pm \frac{1}{2}\delta\mu(\mathbf{r})$,

$$\mathbf{j}_{\uparrow,\downarrow}(\mathbf{r}) = \frac{1}{e\rho_N} \bigtriangledown \mu_0(\mathbf{r}) \pm \frac{1}{2e\rho_N} \bigtriangledown \delta\mu(\mathbf{r}), \tag{2}$$

with μ_0 being the equilibrium, spin independent electrochemical potential in N. μ_0 is either constant or varies linearly with coordinate in regions of non-zero electric field E, where it produces a charge current,

$$\mathbf{j}_q = \frac{1}{e\rho_N} \bigtriangledown \mu_0 = \sigma_N \mathbf{E}.$$

The important prediction of Eq.2 for regions of zero E (outside the path of j_q) is that the current of spin-up electrons is exactly compensated by the opposing current of spin-down electrons, which diminishes the charge flow and doubles the spin flow associated with $\delta\mu$: $\mathbf{j}_\uparrow = -\mathbf{j}_\downarrow, \quad |\mathbf{j}_\uparrow| = |\mathbf{j}_\downarrow|$. For regions of N with non-zero E the spin and charge currents are superposed. The two currents are restricted to the same path only in the pure 1-D case, typical for Giant Magneto Resistance structures [9, 10], but have very different profiles in the general case where the driving electric field is non-uniform in N. To date no experimental evidence exists, which unambiguously verifies spin-charge current decoupling in nanostructures and controversies persist in the analysis of multi-terminal spin based devices [3, 4, 5, 11, 12]. Here we directly demonstrate that spin and charge currents are strictly decoupled in diffusive 1D spin channels.

Johnson and Byers propose an ideal system for demonstrating decoupling of spin and charge currents [11], consisting of a conductive nano-wire with a spin imbalance created by a point injection of a spin-polarized current into the wire and spin-sensitive detectors placed symmetrically about the injection point, which is illustrated in Fig. 1. The fundamental decoupling of the spin and charge currents can be demonstrated by detecting spin signals of *precisely equal strength* in both directions from the injection point while the charge current flows in only one direction. It is essential that the magnetic detectors are closely spaced from the injector within the spin relaxation length in N, ∼100 nm for typical metal films. The detectors are probe tunnel junctions, which should have identical properties. The magnetization states of the detectors must also be arranged by external means to achieve parallel and anti-parallel configurations with respect to the injector. For this 1-D geometry, with a point-like injection at $x = 0$, the solution of Eq.1 is

$$\delta\mu(x) \propto e^{-|x|/\lambda_{sf}}. \tag{3}$$

The spin signal at the detector is a direct measure of $\delta\mu$:

$$V_s = \pm\frac{\gamma}{2e}\delta\mu. \tag{4}$$

This spin signal is compared for the local and non-local case, where the detector is inside and outside the charge current path, respectively. In this letter we report a simultaneous and differential measurement of such local and non-local spin signals, which clearly demonstrates a complete spin-charge decoupling for currents in nanostructures.

Fig. 2 shows a SEM micrograph of the sample fabricated using a two-angle deposition through a lift-off mask, which was patterned by e-beam lithography. The injector and detector junctions are formed by depositing and oxidizing a ∼100 nm wide and 20 nm thick Al strip with a subsequent deposition of 55, 65, and 50 nm wide and 40 nm thick Co electrodes, overlapping the Al strip. The width and thickness of the Al strip are much smaller than the

spin flip length, making it a 1D channel for spin diffusion. The width of the Co electrodes was varied to achieve different switching fields and thereby multiple stable magnetic states of the device. It is essential that the magnetic electrodes switch in a single domain fashion. We found [13] that in such Co based overlap junctions two well defined longitudinal magnetic states with sharp inter-state transitions are obtained for narrow electrodes, 90 nm and less in width. This length is comparable or slightly smaller than the characteristic domain wall size in thin Co. Thin, long, and narrow electrodes can be modelled as single domain particles of uniaxial anisotropy, where the width/length ratio determines the longitudinal switching field. Therefore, the smaller the width the higher the switching field. Such a relation for our geometry is also supported by exact micromagnetic simulations [13]. In order to fine-tune the width of the Co electrodes we have adjusted the layout of the devices such that the total dose during the mask exposure, including the backscattered electrons, was slightly different for the three magnetic electrodes. For example, backscattering is strongest for the center electrode, making it the widest (65 nm) of the three and therefore with the lowest switching field (1.13 kOe). The outer Co electrodes were 50 and 55 nm wide with the switching fields of 1.62 and 1.45 kOe, respectively.

The measurements have been done using a standard lock-in technique at 7 Hz, which we found necessary for achieving $\sim 0.1\%$ level resolution in the spin signal measurements. The ac technique resulted in a weak but non-zero inductive crosstalk between the injection and detection circuits, which scaled to zero with decreasing the excitation frequency. This small constant background of $\sim$ 30 nV had no influence on the spin-dependent signals studied, which was verified by measuring the latter at different frequencies as well as a dc technique. The external field was applied along the length of the Co electrodes. The sample was electrically characterized as follows: injecting the current from probe 3 to probe 4 (I_{34}), we measure the non-local voltages V_{10} and V_{20} at two distances from the injection point. In this non-local measurement configuration, the voltage probes are outside the current path.

According to Eqs. 3,4 the ratio of these voltages for our 1-D geometry is

$$V_{10}/V_{20} = \exp(d_{12}/\lambda_{sf}), \tag{5}$$

where $d_{12} = 300$ nm is the electrode separation and $\lambda_{sf} = \sqrt{D\tau_{sf}}$ is the spin diffusion length, found to be 850 nm at 4 K. Here D and τ_{sf} are the diffusion constant and spin relaxation time, respectively. The diffusion constant was calculated from the measured resistivity of the wire, $\rho = 4.0$ $\mu\Omega$cm, using the Einstein relation $D = [e^2\rho N(E_F)]^{-1} = 65$ cm^2/s, where e is the electron charge and $N(E_F) = 2.4 \times 10^{28}$ eV^{-1}m^{-3} is the density of states of Al at the Fermi energy [15]. The resulting spin relaxation time is $\tau_{sf} = 110$ ps, much longer than the Drude scattering time, $\tau_p/\tau_{sf} \sim 10^{-4}$. From the measured spin voltages we can also determine the effective spin polarization $P = 12\%$ ($V_{i0} \propto P^2$ [11]). These values are in good agreement with the recent spin injection studies on Al films [5, 14] but differ from the early single crystal Al data [1, 16] due to stronger impurity and surface scattering in thin films.

In Fig. 3a the local spin signal (V_{30}, solid line) and the non local spin signal (V_{10}, dashed line) are plotted as a function of the applied magnetic field, for I_{42}=5 μA. Isotropic spin diffusion necessarily results in these two spin voltages being identical in magnitude. A precondition is that the detectors have the same physical characteristics, such as polarization, which is achieved in our case by the simultaneous deposition of all three junctions. The switching of the injector electrode at 1.13 kOe ($\downarrow\downarrow\downarrow \rightarrow \downarrow\uparrow\downarrow$) reverses the sign of the injected spin population in the wire. This is measured simultaneously by the two detectors and yields *exactly* the same spin voltages, thus demonstrating that the spin currents are identical in both directions while the charge current flows only in one direction. As the field is increased, detector 1 switches ($\downarrow\uparrow\downarrow \rightarrow \uparrow\uparrow\downarrow$), followed by a switching of the second detector ($\uparrow\uparrow\downarrow \rightarrow \uparrow\uparrow\uparrow$), again demonstrating the symmetry in the spin current.

An even more direct demonstration of the effect is the differential spin signal (V_{13}) shown in Fig. 3b, which, in addition to eliminating the fabrication related uncertainties, also rules

out possible measurement errors, such as small differences in gain and drift of the separate amplifiers and small spin misalignments in the junction areas. The raw differential signal V_{13} contains the resistive, spin-*independent* contribution from V_{23} ($V_{23}/I_{42} = 6\ \Omega$) as well as both spin-*dependent* signals from V_{30} and V_{10}. The switching of the injector at 1.13 kOe ($\downarrow\downarrow\downarrow \rightarrow \downarrow\uparrow\downarrow$) leaves the differential spin voltage unchanged to within the experimental uncertainty of $< 1\%$ (Fig. 3b), while the two component signals change by the maximum amount (Fig.3 a). The slight skew in the signals in Fig. 3a,b as the reversing field is increased is connected with small spin perturbations in the junction areas caused by the opposing external field ($<$1.65 kOe). We emphasize however, that the power of our symmetric detection scheme is in eliminating this micromagnetic uncertainty. The change of the magnetic state of the injector at a given point in field (1.13 kOe) changes both spin signals by the same maximum amount. However, the magnetic states of the detector electrodes, even if slightly misaligned, are not affected by this instantaneous switching of the injector. The differential signal therefore remains unchanged (Fig. 3b at 1.13 kOe).

A difference in width for the two detector electrodes was necessary to separately control the respective magnetic states by an external magnetic field. The small uncertainty this introduces can be estimated as follows. From Eqs. 3,4,5 the variation in detector width from 50 to 55 nm can be estimated to produce a 0.06% change in the detector voltage. A change in the detector width of even a factor of 2 (50 nm to 100 nm) would still have a very small effect on the the effective spin signal detected ($\sim 0.1\%$). The uncertainty due to the difference in width of our two detectors (5 nm) is thus negligible, determined by the relatively large scale set by the spin diffusion length. The relative weight of the detector placement error is on the other hand larger, and follows directly from Eq. 5. Our experimental placement error for the sample discussed above is approximately 5 nm corresponding to a 0.6% change in the detector voltage, which is still within the $\sim 1\%$ precision we report. We have measured several samples with well controlled magnetic switching and similar geometrical uncertainties, all confirming the above result at the 1% level.

In summary, we use a multi-terminal spintronic device to unambiguously verify the complete decoupling of spin and charge currents in the regime of diffusive transport. The important consequence of this decoupling is that numerous recently proposed multi-terminal spin-based devices should benefit in sensitivity by use of non-local as opposed to local spin currents.

Acknowledgements

Financial support from the Swedish Foundation for Strategic Research (SSF) is gratefully acknowledged.

Figure captions:

Fig.1 Schematic of the mechanism of spin and charge transfer for a current injected from a ferromagnet (electrode "2") into a non-magnetic conducting wire. The spin current is symmetric about the injection point and is due to opposing currents of spin-up and spin-down electrons (see Eq. 1). The density of the spin current (J_s, grey shaded) decays exponentially from the injection point. The charge current is asymmetric and unpolarised, (J_q, white). The density of the charge current is uniform between the injector (Inj) and ground (G). The injected non-equilibrium spin accumulation can be sensed by ferromagnetic detectors in the vicinity of the injection point (electrodes "1" and "3") either with respect to the floating end of the nano-wire (F) or differentially.

Fig.2 SEM micrograph of the sample consisting of an oxidized 100 nm wide and 15 nm thick Al strip overlapped by three 40 nm thick Co electrodes of 55, 65, and 50 nm in width. The junction resistances are $\sim 20\ k\Omega$. The injection-detection configuration for non-local and differential (local versus non-local) measurement configurations is indicated.

Fig.3 a) local (solid) and non-local (dashed) spin signals measured simultaneously as a function of external field. b) differential signal as a function of field. The constant, spin-*independent* resistive offset ($V_{23}/I_{42} = 6\ \Omega$) has been subtracted from the raw V_{30} and V_{13} signals, allowing a direct comparison of the spin-dependent signals. The behavior in negative fields is identical. The ~ 30 nV offset in V_{10}, V_{30} is due to a spin-independent inductive crosstalk (see text). All data were taken at 4 K with $I_{42} = 5\ \mu$A. The arrows indicate the magnetization states of the three ferromagnetic electrodes.

References

[1] Johnson, M.; Silsbee, R. H. *Phys. Rev. Lett.* **1985,** 55, 1790.

[2] Zutic, I.; Fabian, J.; Das Sarma, S. *Rev. Mod. Phys.* **2004,** 76, 323.

[3] Jedema, F. J.; Filip, A. T.; van Wees, B. J. *Nature* **2001,** 410, 345.

[4] Johnson, M. *Nature* **2002,** 416, 809 .

[5] Jedema, F. J.; Filip, A. T.; van Wees, B. J. *Nature* **2002,** 416, 810.

[6] Sharma, P. *Science* **2005,** 307, 531.

[7] Kato, Y. K.; Myers, R. C.; Goussard, A. C.; Awschalom, D. D. *Science* **2004,** 306, 1910.

[8] Aronov, A. G. *JEPT Lett.* **1976,** 24, 32.

[9] van Son, P. C.; van Kempen, H.; Wyder, P. *Phys. Rev. Lett.* **1987,** 58, 2271.

[10] Valet, T.; Fert, A. *Phys. Rev. B* **1993** 48, 7099.

[11] Johnson, M.; Byers, J. *Phys. Rev. B* **2003,** 67, 125112.

[12] Jedema, F. J.; Nijboer, M. S.; Filip, A. T.; van Wees, B. J. *Phys. Rev. B* **2003**, 67, 085319.

[13] Urech, M.; Korenivski, V.; Haviland, D. B. *J. Appl. Phys.* **2002,** 92, 6062.

[14] Valenzuela, S. O.; Tinkham, M. *Appl. Phys. Lett.* **2004,** 85**,** 5912.

[15] Papaconstantopoulos, D. A. *Handbook of the Band Structure of Elemental Solids;* Plenum: New York, 1986.

[16] Lubzens, D.; Schultz, S. *Phys. Rev. Lett.* **1976,** 36, 1104.

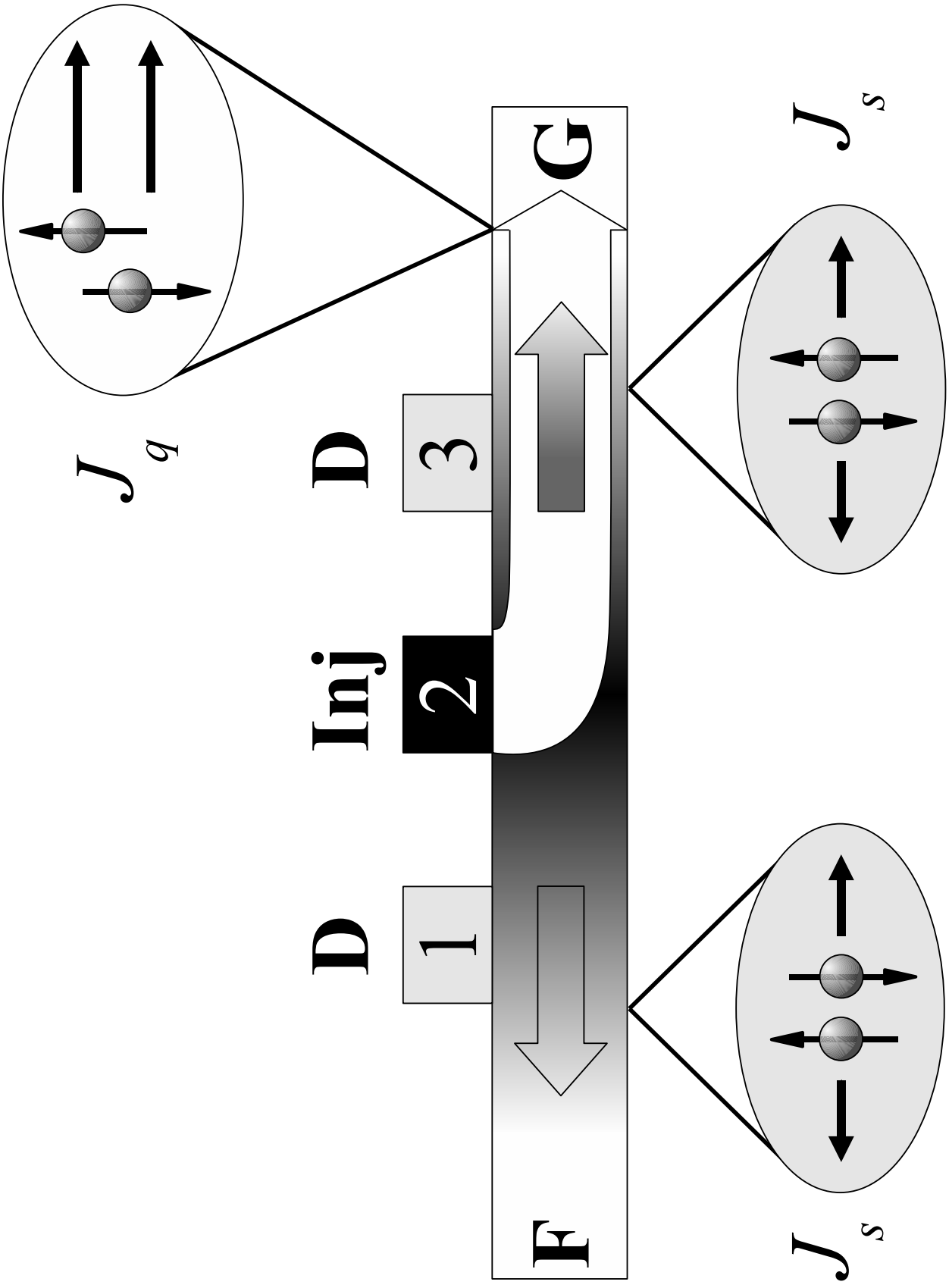

Fig. 1: Urech *et al.*

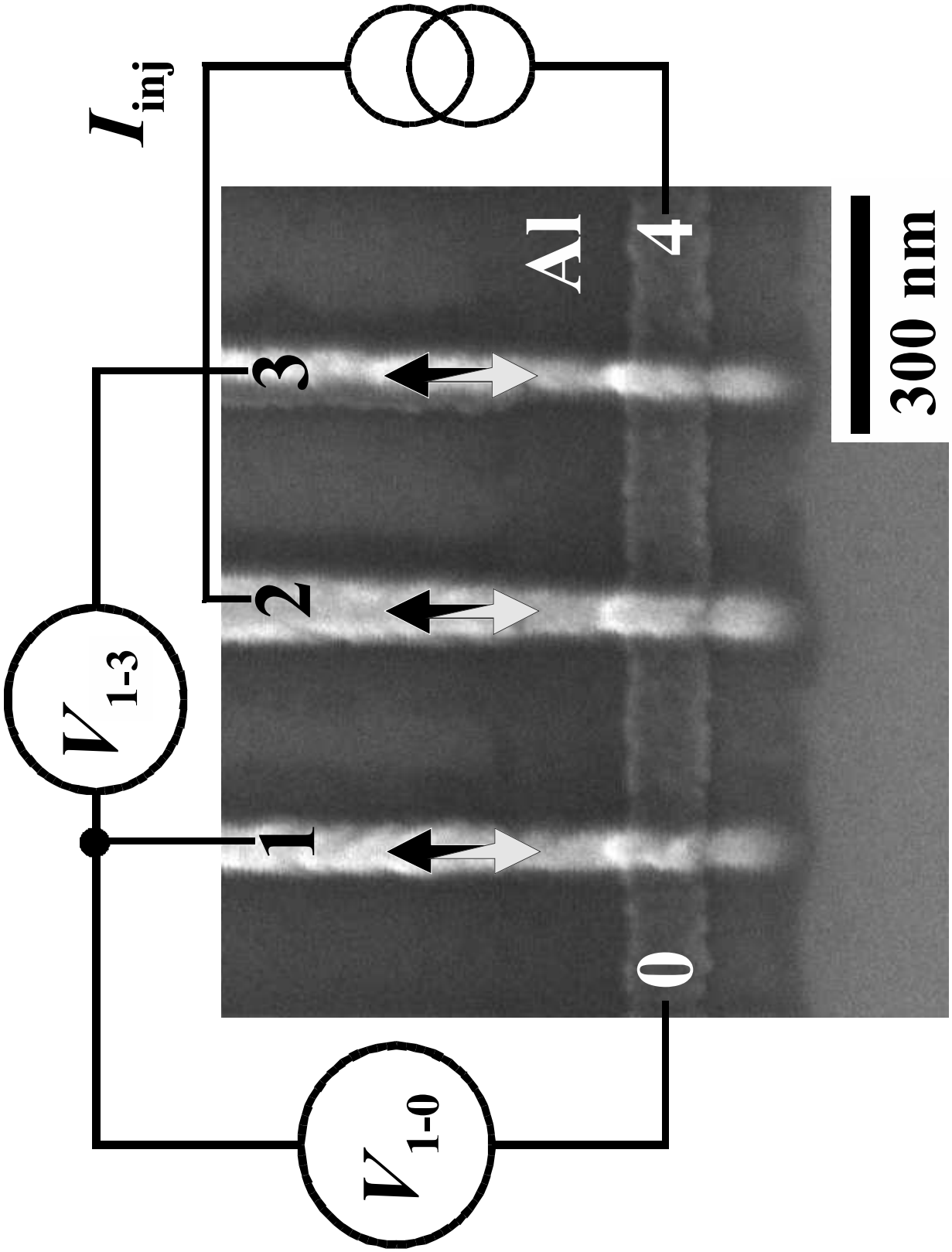

Fig. 2: Urech *et al.*

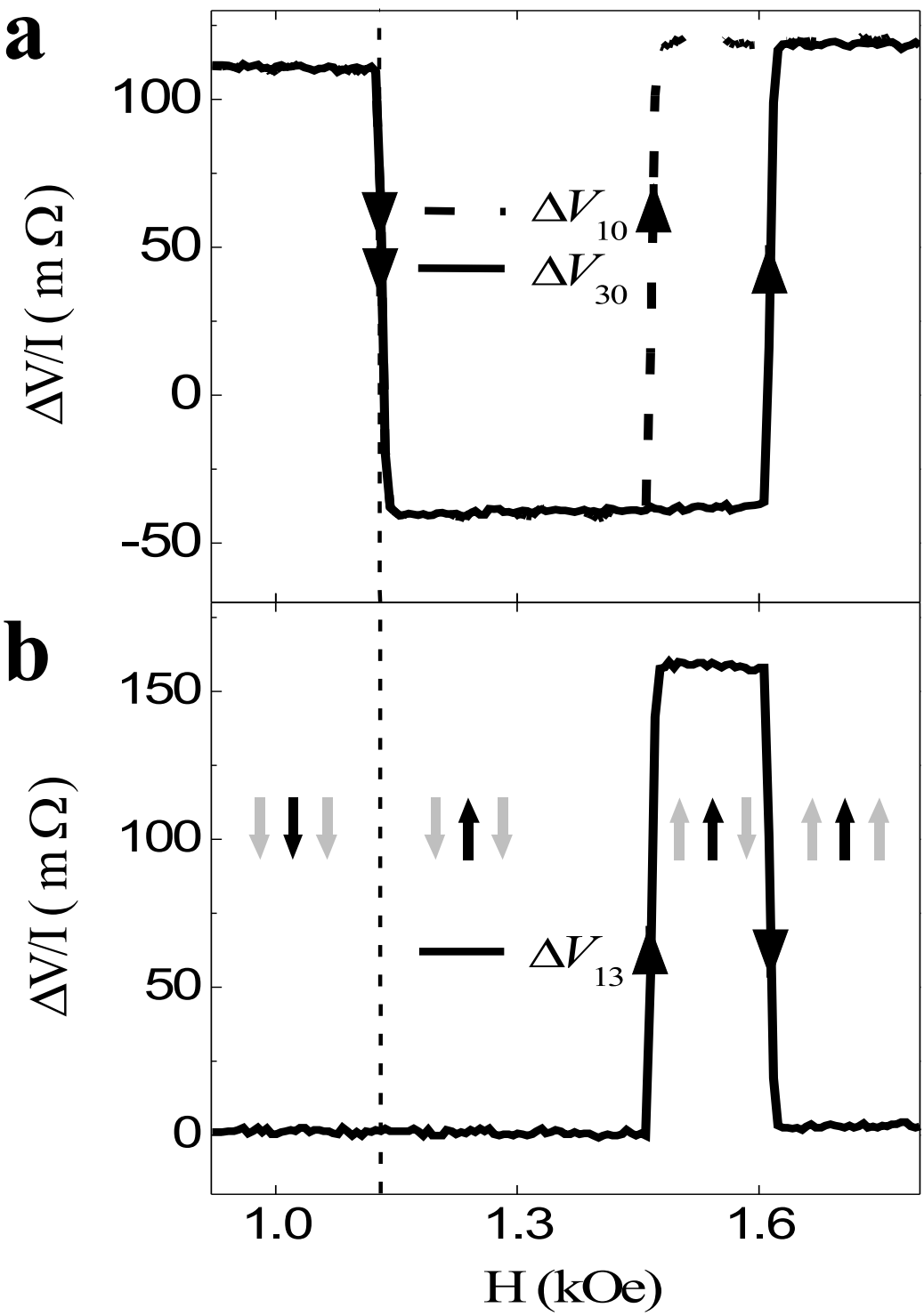

Fig. 3: Urech *et al.*